HHS Public Access

Author manuscript

Math Geosci. Author manuscript; available in PMC 2015 July 15.

Published in final edited form as:

Math Geosci. 2013 August ; 45(6): 681–704. doi:10.1007/s11004-013-9474-1.

Time-Lapse Analysis of Methane Quantity in the Mary Lee Group of Coal Seams Using Filter-Based Multiple-Point Geostatistical Simulation

C. Özgen Karacan and

NIOSH, Office of Mine Safety and Health Research, Pittsburgh, PA 15236, USA

Ricardo A. Olea

USGS, Eastern Energy Resources, Reston, VA 20192, USA

C. Özgen Karacan: cok6@cdc.gov

Abstract

Coal seam degasification and its success are important for controlling methane, and thus for the health and safety of coal miners. During the course of degasification, properties of coal seams change. Thus, the changes in coal reservoir conditions and in-place gas content as well as methane emission potential into mines should be evaluated by examining time-dependent changes and the presence of major heterogeneities and geological discontinuities in the field. In this work, time-lapsed reservoir and fluid storage properties of the New Castle coal seam, Mary Lee/Blue Creek seam, and Jagger seam of Black Warrior Basin, Alabama, were determined from gas and water production history matching and production forecasting of vertical degasification wellbores. These properties were combined with isotherm and other important data to compute gas-in-place (GIP) and its change with time at borehole locations. Time-lapsed training images (TIs) of GIP and GIP difference corresponding to each coal and date were generated by using these point-wise data and Voronoi decomposition on the TI grid, which included faults as discontinuities for expansion of Voronoi regions. Filter-based multiple-point geostatistical simulations, which were preferred in this study due to anisotropies and discontinuities in the area, were used to predict time-lapsed GIP distributions within the study area. Performed simulations were used for mapping spatial time-lapsed methane quantities as well as their uncertainties within the study area.

The systematic approach presented in this paper is the first time in literature that history matching, TIs of GIPs and filter simulations are used for degasification performance evaluation and for assessing GIP for mining safety. Results from this study showed that using production history matching of coalbed methane wells to determine time-lapsed reservoir data could be used to compute spatial GIP and representative GIP TIs generated through Voronoi decomposition. Furthermore, performing filter simulations using point-wise data and TIs could be used to predict methane quantity in coal seams subjected to degasification. During the course of the study, it was shown that the material balance of gas produced by wellbores and the GIP reductions in coal seams predicted using filter simulations compared very well, showing the success of filter simulations for continuous variables in this case study. Quantitative results from filter simulations

Correspondence to: C. Özgen Karacan, cok6@cdc.gov.

of GIP within the studied area briefly showed that GIP was reduced from an initial ~73 Bcf (median) to ~46 Bcf (2011), representing a 37 % decrease and varying spatially through degasification. It is forecasted that there will be an additional ~2 Bcf reduction in methane quantity between 2011 and 2015. This study and presented results showed that the applied methodology and utilized techniques can be used to map GIP and its change within coal seams after degasification, which can further be used for ventilation design for methane control in coal mines.

Keywords

Coal seam degasification; Coalbed methane; Coal mine methane; Multiple-point geostatistics; Filter simulation; Training image

1 Introduction

Current US regulations prohibit methane concentrations exceeding 1 % in an underground coal mine and 2 % in bleeder systems. Ventilation of underground coal mines with an adequate amount of diluting airflow is important in order to prevent formation of explosive methane-air mixtures. Coal-seam degasification prior to coal mining is an indispensable practice for reducing gas-in-place (GIP) in the coal and thereby for supplementing ventilation to control methane emissions during mining (Dougherty and Karacan 2011; Karacan et al. 2011). Effectiveness of degasification wells can be influenced by fluid-flow- and fluid-storage-related reservoir properties of coal seams. From a field perspective, a degasification plan should take the structural geology of the field and presence of multiple seams and their reservoir conditions into account in order to be effective. These seams can be overlying and underlying the main seam in a coal group and can act as potential sources of floor and roof emissions, respectively, during mining. Additionally, presence of major faults should be taken into consideration as they may affect uniform degasification of the field by creating reservoir compartmentalization (Karacan 2008). During degasification, reservoir properties of coal seams change. Therefore, determining temporal coal reservoir properties at spatial well locations are important for predicting high-flow-capacity areas of the reservoir and for estimating GIP and its change with time. Equally if not more important is the ability to determine the remaining GIP at intervening spaces between wellbores. This ability can greatly help assessing spatial locations of potential methane emissions into mines from different seams of the coal group and evaluating the locations of infill wells to remove additional gas to improve miner safety (Karacan 2008; Karacan et al. 2012).

Currently, GIP computations related to degasification performance in a coal seam and coal mine methane management objectives are performed by running laboratory tests on cores in order to determine gas content and sorption isotherms. GIP is then calculated for a unit volume of the coal seam based mainly on absorbed quantity by excluding free gas quantity since calculation of free gas requires porosity and water saturation data. In most cases, cores or laboratory analyses are not available for the spatial location of interest. In such instances, GIP in the area is assumed uniform based on calculations at a close location, if they exist. Current approaches to determine GIP is neither exact, nor provides information as to how it has changed in time and may change in the future. This paper presents a unique case study

and a novel approach demonstrated for the first time for spatially quantifying time-lapsed changes in GIP and its uncertainty through the use of production history matching and multiple-point geostatistics in a 12,900-acre area in Black Warrior Basin, Alabama (Karacan 2013a). Since production history matching is the study of mimicking actual water and gas production data from wellbores by using theoretical solutions of flow and fluid storage in a reservoir, it can be used for determining coal reservoir properties, which can further be used to determine point-wise volumetric GIP at wellbore locations. This study is also the first to employ TIs (which were generated by using a systematic approach for coal seam degasification) and filter simulations for spatial modeling of time-lapsed GIP and its changes in multiple coal seams mining area in order to assess emission potentials from different horizons. This study was conducted in an area where both degasification and coal mining takes place in the Mary Lee coal group; that is, the New Castle, Mary Lee, Blue Creek, and Jagger coal seams. Time-varied reservoir properties of coals for initial (1987 and before), 1998, 2006, 2011, and 2015 time periods obtained from production history matching and rate forecasting (for 2015) of gas and water production from 86 degasification wells were used to compute GIP and its change at spatial well locations. These data were used to generate separate TIs at each date and for each coal seam using Voronoi decomposition to create a total of 27 TIs, which later were tested for their statistical and spatial representativeness of the original spatial data. Time-lapsed GIP data of each coal seam were stochastically simulated using filter-based geostatistical simulation that was specifically used in this work due to anisotropies and the presence of horst and graben-type normal faults, and also to capture the discontinuities they create as patterns with the help of TIs.

2 Study Area Description and the Procedure Leading to Geostatistical Simulations

In this paper, the intent is to calculate GIP and its time dependent changes in the Mary Lee group of coals for mapping these properties in the study area. However, for completeness, the background material is briefly described in the upcoming sections.

2.1 Mary Lee Coal Group of the Black Warrior Basin and the Specific Study Area

The Black Warrior basin is structurally complex, having multiple faults and fractures within the study area. The Black Warrior basin contains numerous northwest striking normal faults and joints which form horst and graben structures with displacements as much as 400 ft (McFall et al. 1986). Structural deformation in the general area is known to have a significant effect on the performance of coalbed methane wells, mining emissions, and hydrodynamics (Pashin 2007; Groshong and Pashin 2009; Pashin 2010). The majority of the Black Warrior basin coal-bearing strata of economic value are in the Pennsylvanian age Pottsville formation. In the Upper Pottsville formation, the Mary Lee coal group is most important due to ongoing coal mining and coal gas production activities. The Mary Lee coal group covers an interval of about 250 ft thick and includes the New Castle, Mary Lee, and Blue Creek and Jagger seams (Fig. 1). During coal mining, the Mary Lee and Blue Creek seams are usually mined together in areas where the parting layer is thin. Therefore, in this

work, they will be treated as a single coal unit, excluding thickness of parting, and will be termed as the Mary Lee/Blue Creek seam.

The coal mine located within the study area has recently started operating with the E1 panel (Fig. 2) in the Mary Lee coal group to extract the Blue Creek and Mary Lee seams (with a total thickness varying between 4 and 10.9 ft, and a mean of 6.6 ft) by longwall method. In the study area, the New Castle seam is at most 65 ft and the Jagger seam is at most 41 ft above and below the mining interval, respectively. These two seams will be within the fractured interval at the roof and floor of the mine during mining and after the panels are sealed, and will be potential methane emission sources from the roof and floor through mining-induced fractures. Therefore, the amount of methane in the mined seams, as well as in the New Castle and Jagger seams are important for predicting emissions during mining in order to effectively plan ventilation needs for mining safety.

2.2 Study Area, Production History Matching of Degasification Wells and Gas-in-Place

The study area, shown in Fig. 2, has 86 vertical boreholes, some of which started production as early as 1987. The majority of the wellbores have been in production since their start date, for about 6,000 days.

Figure 2 shows that there are five major fault lines in the study area. Mine panels are designed to take fault lines into consideration. It is not clear whether these faults are permeable or impermeable for cross flow or for vertical flow along the fault lines. The data, however, shows that the area is faulted as a horst and graben structure, and the blocks between faults are down-thrown with varying vertical distances up to 200 ft. These structural faults are not expected to have major impact on initial gas accumulation within the coal seams. However, with vertical displacements as much as 200 ft, it is clear that the faults are discontinuities for strata and for coal seams, and thus they may affect degasification efficiency of wells, decline rates, coal seam pressures, and gas quantity changes on both sides of faults during different stages of degasification (Karacan 2013a). As a result, longwall panels located at different positions with respect to fault lines and fault blocks may experience different levels of methane emissions as well (Karacan 2008, 2011).

Production history matching analyses of vertical degasification wells used in this study were completed using Fekete's F.A.S.T. CBM™ software version 4.7 (Fekete Associates 2012). For modeling, pseudo-steady state (PSS) boundary-dominated solution—which ignores the initial transient period and assumes that effective drainage radii reached its boundaries—was used. For wellbores produced for so long, as the ones in this field, this is an acceptable assumption to analyze their production behavior. Production history matching is the study of production behavior of wellbores by using theoretical solutions of fluid flow and storage in a reservoir, developed for different boundary conditions. The main purpose of production history matching is to predict reservoir properties by using other ancillary information, such as geophysics, and expert knowledge regarding the flow regimes. In order to obtain reliable results though, completion parameters and production intervals of the wellbores as well as the geometry of the solution domain should be represented realistically. For each well and coal group, well productions were simulated starting from their first reported production date. Since the degasification start date (or production start date) of each well could be

different and are usually before 1987, the first date that defines the initial conditions of the coal seams predicted from each of the wellbores is termed initial in results in order to refer to the initial reservoir condition of coal seams prior to the start of degasification. Time-dependent reservoir properties, as appropriate, were determined using history matching results for initials (prior to start of degasification), 1998, 2006, 2011, and 2015 (which was based on production forecasting) for all wells. Details of production history matching process can be found in Karacan (2013a). History matching of well productions through a PSS boundary-dominated solution enabled the prediction of reservoir properties of the New Castle, Mary Lee/Blue Creek, and the Jagger seams and their changes though time. These properties, in combination with isotherm measurements, could later be used for computation of volumetric GIP (absorbed and free gas) in individual seams at a given time (t) through volumetric GIP computation equations given in Saulsberry et al. (1996) and in Karacan (2013b). The change in GIP quantity at a given location between two time intervals due to degasification was obtained by subtracting the corresponding values of GIP.

The GIP calculations were performed for the model grids in which wellbores are located (a 0.92-acre area) corresponding to each of the 86 degasification wells. Tables 1 and 2 give statistical measures of GIP calculations for borehole locations at all dates and the differences of GIP between consecutive dates, respectively. The statistical measures of differences given in Table 2 can be interpreted as the statistics of reduction in GIP at 86 wellbore locations due to degasification. From a mining-related methane-emissions point of view, the univariate statistical GIP data given in Table 1 refer to the potential amount of methane entering into the mine from the roof (New Castle), mined seam (Mary Lee/Blue Creek), and floor (Jagger) at a given date when 0.92 acres of Mary Lee/Blue Creek seam is mined, if GIP is assumed to be constant throughout the study area. Likewise, the GIP reduction statistics given in Table 2 refer to the reduction in methane quantity when 0.92 acres is mined. However, although point-wise data and evaluation of GIP and GIP differences can be helpful, this approach is average and does not present spatial differences between data locations. In the forthcoming sections, filter-based geostatistical simulation that was used in this work to establish spatial correlations and continuity and to assess the uncertainty of GIP and GIP difference data are discussed. Geostatistical modeling and simulations were conducted over the study area presented in Fig. 2.

3 Filter-Based Multiple-Point Geostatistical Simulation of Time-Lapsed Gas-in-Place

The theory and in-depth review of geostatistical techniques and examples are given in Journel et al. (1998), Deutsch and Journel (1998), Webster and Oliver (2007), Leuangthong et al. (2008), Remy et al. (2009), Olea (2009), Wackernagel (2010), and Srivastava (2013). These techniques have been widely used for coal resource evaluation and mining also (Heriawan and Koike 2008; Olea et al. 2011; Karacan et al. 2012; Karacan and Goodman 2012; Olea 2013). However, most of these examples used variogram techniques, which cannot reproduce complex patterns, discontinuities, and curvilinear shapes (Zhang 2008). Multiple-point statistics (mps) proposed by Journel (1992) and extended by Guardiano and Srivastava (1992) by the use of a training image (TI), were made practical with SNESIM

(Strebelle 2000) and SIMPAT (Arpat and Caers 2007) and FILTERSIM (Zhang et al. 2006) algorithms (Wu et al. 2008a). In this work, Stanford Geostatistical Modeling Software's (SGeMS) implementation of FILTERSIM was employed to simulate time-lapsed GIP and time-lapsed differences in GIP in the New Castle, Mary Lee/Blue Creek, and Jagger seams. FILTERSIM and its SGeMS implementation are discussed in detail in Wu et al. (2008b) and in Remy et al. (2009). Therefore, the simulation technique will not be reiterated in this paper. However, it is important to mention that the FILTERSIM application has been chosen in this work due to strong anisotropies in the data (represented by semivariograms) and also its ability to include the faults in the study area and their effects in the simulations, where the kriging system of equations would create singularity due to discontinuities.

3.1 FILTERSIM Technique and Its Application in This Work

3.1.1 Generating and Testing Training Images—Geostatistical modeling is based on 86 GIP data points, whose time-dependent statistics are given in Tables 1 and 2. GIP and GIP differences were simulated separately instead of subtracting (or adding) grid cell values of realizations to avoid propagation of simulation errors. The spatial data locations are the well locations shown in Fig. 2 as full circles with well numbers. For modeling, the data was assigned to simulation grids that had 115 × 122 Cartesian grids, in which each grid was 200 ft in *x*- and *y*-directions, respectively, to give a grid area of 0.92 acre. Thus, simulation grids had 14,030 grid cells and represented a total area of 12,900 acres shown in Fig. 2.

Multiple-point simulation aims to capture patterns or structures from training images (TI) and condition them to local data in pattern classification and simulation. Although TI can be conceptual and does not have to honor the data patterns precisely in the FILTERSIM application, it is suggested to use realistic training images (Olea 2009). However, there are not any strict rules regarding generation of TIs for continuous variables. In this work, the aim was for statistical and spatial representation of data and the presence of geological features in the 27 TIs that corresponded to each of the cases in Tables 1 and 2. For this purpose, 27 TI grids of the same dimensions and grid counts as the simulation grids were created. Fault lines were placed into each of the grids as discontinuities based on their spatial locations corresponding to Fig. 2. For TI generation, first-order Voronoi decomposition was employed as: Let S be a set of n distinct points, s_i, $\forall_i \in n$. The Voronoi diagram of S is the partition of the plane into n regions, $R(s_i)$. A point equal to s_i is assigned to q in $R(s_i)$ if $||q - s_i|| < ||q - s_j||$, for each $s_j \in S$, $i \neq j$. For equally spaced data in Euclidian space, Voronoi decomposition creates square regions. However for random data, the plane S is partitioned into polygons (Voronoi regions) in such a way that each region contains exactly one generating point and every point in a given region is closer to its generating point than to any other. Faults, represented as discontinuities in Voronoi decomposition prevented expansion of Voronoi regions beyond fault lines. In this work, Surfer™ 10 (Golden Software 2012) was used for Voronoi decomposition. Besides being used in many applications in computer sciences, geological sciences, and atmospheric sciences (Mackie and Cooper 2009), Voronoi decomposition of hard data (spatial GIP and GIP difference data) as Voronoi diagrams offers a unique advantage in this work in preparing TIs; as explained in the upcoming section (Sect. 3.1.2), K-means clustering was used in filter simulations in this work due to its benefits in partitioning the data into clusters for stochastic

simulations (Remy et al. 2009). However, the major problem with K-means clustering is that it cannot ensure the global optimum results due to the random selection of initial cluster centers. Clustering the data using K-means with the help of Voronoi diagrams ensures effective selection of initial cluster centers compared to random initialization (Reddy and Prasanta 2012).

Figure 3 shows initial GIP and GIP difference (1998–2006) of data and their TIs generated for the Jagger seam as examples. All TIs prepared as Voronoi diagrams for each case were examined by comparing their statistics with those of actual data using basics statistics and Quantile–Quantile (Q–Q) plots. Q–Q plots were prepared between 86 values of actual data and 14,030 grid cell data of TIs for each coal seam and for each time-dependent attribute. A straight line in Q–Q plots is an indication of equality between the probability distributions being compared. Tables 3 and 4 give basic statistics of TI images for comparison with statistics of actual data at borehole locations given in Tables 1 and 2. Comparison of statistical parameters in these table pairs (1 versus 3, and 2 versus 4) shows that the values in these tables for corresponding time-dependent GIPs are very close to each other, indicating statistical similarity and representativeness of TIs to the actual data. Q–Q plots of the actual data-TI map pairs shown in Fig. 3, as examples, also show that the distributions have similar quantile values (Fig. 4A for GIP and B for GIP difference). The inset tables provided in these figures show the mean and variance of the original data and the TI data used for Q–Q comparisons.

Additionally, spatial aspects of the data-TI pairs were tested for spatial representativeness. For this purpose, semivariogram analyses were performed on the data-TI pairs without any data transformation. It should be emphasized that filter simulation does not require semivariogram modeling. Semivariogram was used here for the sole purpose of comparing spatial distributions of actual data with the distribution TI data generated from them. Also, since vertical spatial modeling is not sought after for this purpose, horizontal semivariograms are appropriate for assessing spatial similarity of data-TI pairs. Figure 5 shows the isotropic experimental semivariograms calculated using 900 ft lag distance, and the analytical models, of the initial GIP data for the Jagger seam and its TI (shown in Fig. 3) as an example. The isotropic experimental semivariogram of the data at borehole locations were represented with an exponential model (Eq. (1)). The dotted lines in Fig. 5 show the total variance in each of the data.

That is,

$$\gamma(h)=C_o+C\left[1-\exp\left(\frac{-h}{A_o}\right)\right], \quad (1)$$

where $\gamma(h)$ is the semivariance, h is the lag, C_o is the nugget variance, C is the sill contribution, and A_o is the range parameter, which is 1⁄3 of the effective range (A) in the case of exponential model. Effective range, A, is where the sill ($C + C_o$) is within 5 % of the asymptote (Gamma Design Software 2008). The analytical model representing spatial data at borehole locations had 0.00117 nugget variance (C_o) and 0.05040 sill variance ($C_o + C$). It had a range parameter (A_o) of 3140.7 ft and an effective range (A) of 9422 ft. The

experimental variogram of the TI was calculated with the same parameters as those of the borehole-location data, and the analytical model was plotted using same model parameters. Figure 5 shows that both actual data and its TI data present similar semivariograms and can be closely modeled using the same models. However, as expected, the TI has lower variance owing to the large number of data. Similar comparisons presented for Jagger seam's initial GIP at borehole locations and the TI in this section were performed for other data-TI pairs as well. It was concluded that the Tls prepared using Voronoi decomposition can represent the actual data statistically and spatially, at least for the case study presented in this work.

3.1.2 Implementation of Filter Simulation for This Work—Filter simulation operates by capturing features and patterns from TIs by running a set of filters, which are basically weights associated with a search template (Wu et al. 2008a). SGeMS implementation of FILTERSIM offers three default filters as average filter, gradient filter, and curvature filter to create filter scores from TIs, where similar patterns are associated with similar vector scores through clustering. These default filters are given as (Remy et al. 2009)

$$f_1^i(\alpha_i)=1-\frac{|\alpha_i|}{m_i}\in[0,1];\quad \text{Average filter}, \tag{2}$$

$$f_2^i(\alpha_i)=\frac{\alpha_i}{m_i}\in[-1,1];\quad \text{Gradient filter}, \tag{3}$$

$$f_3^i(\alpha_i)=\frac{2|\alpha_i|}{m_i}-1\in[-1,1];\quad \text{Curvature filter}. \tag{4}$$

If all is selected, which was the case in this work, these filters operate in each of the template directions of the study geometry by sliding the filter nodes. For instance, for a two-dimensional template of *X*–*Y* directions, there will be six filters. In these filter definitions, n_i is the template size in *i* direction, which can be *X* or *Y*. The term m_i is $(n_i - 1)/2$ with a filter node offset of $\alpha_i = -m_i, \ldots, +m_i$. Filters are the crucial elements for creating score maps, from which local training patterns are summarized in filter score space. By partitioning filter scope space into similar patterns that can be grouped together, pattern prototypes (*prot*) is calculated by point-wise average of all training patterns (*pat*) that fall into a specific class (Remy et al. 2009). For a continuous training image, a prototype associated with search template T_J is calculated using

$$prot(\mathbf{h}_i)=\frac{1}{c}\sum_{j=1}^{c} pat(\mathbf{u}_j+\mathbf{h}_i),\quad i=1,\ldots,J. \tag{5}$$

In this equation, $\mathbf{h}_i$ is the *i*th offset location for the filter in the search template T_J, *c* is the number of training replicates within the prototype class, and $\mathbf{u}_j$ is the center of a specific training pattern. The structure and properties of filters, as well as pattern identification and clustering methodologies are explained in detail in Remy et al. (2009). One other note of interest here regarding the successful implementation of filter simulation procedure, besides

representativeness of TIs, is that the pattern identification and prototype building are dependent also on template search and simulation parameters. In this work, FILTERSIM simulations were conditioned to hard data only and have not been forced to match the TI histogram to create realizations. However, simulation parameters including the number of clusters, clustering method, search template, and patch dimensions can affect the results. Therefore, a deductive reasoning approach was used in such a way that these parameters were optimized by trying different combinations and checking the data of Q50 realizations against the data of TIs, as well as against the hard data of well locations using Q–Q plots (Fig. 4A–C and Fig. 4B–D and their inset tables) and basic statistics (Tables 1 and 3, and Tables 2 to 4). Eventually, a two-dimensional search template with 5 cells in *x*–*y* directions and inner patch dimensions with 3 cells in *x*–*y* directions were chosen. Pattern partition was performed using K-means clustering. In K-means clustering, the optimal centroid of each cluster is associated with specific training patterns based on the distance between patterns and cluster centroids (Wu et al. 2008a, 2008b). For this operation, 22 maximum initialization clusters and 2 secondary partition clusters were selected. As the distance calculation method, filter scores were used. After parameter optimization for FILTERSIM, one-hundred realizations for each of the time-lapse GIP and time-lapse GIP difference data for each coal seam were generated. This set of simulations was used for analyses of uncertainty and distribution of properties in the study area.

3.2 Evaluation of Time-Lapsed Gas-in-Place and Time-Lapsed Gas-in-Place Difference Realizations

Filter simulations that use a stochastic approach generated 100 realizations for each of the GIP and GIP-change cases for the New Castle, Mary Lee/Blue Creek, and the Jagger seams; therefore, in total, 27 × 100 realizations, each having 14,030 grid cell values, were generated for all cases to build time-lapsed results. One hundred realizations of each of the 27 cases were used to perform probabilistic assessment of GIP and also to rank the realizations to determine the ones that represent the Q50 ones as expected maps.

3.2.1 Material Balance Between Simulated Realizations and Cumulative Borehole Productions—Before proceeding with evaluations of GIP values in realizations from filter simulations and grid cell values within, a global material balance check was performed between amount of gas produced from degasification wellbores and the amount of GIP reduction in coal seams. Although the gas produced from wells comes to the surface from a single point, or grid cell, in reality it sources from a volume around the wellbore. Thus, cumulative gas production from the Mary Lee group’s coal seams via degasification wells should reflect the amount of GIP reduction in all the Mary Lee group’s coals within the study area. For this purpose, GIP and GIP difference realizations of all coals were ranked based on cumulative grid cell values and Q5, Q50, and Q95 were found. Rankings corresponding to each coal seam were summed together to find cumulative methane quantity change between initial and later dates. These values were compared with the amount of gas produced from the Mary Lee group by degasification wells. Results are given in Figs. 6A and 6B. These figures show that cumulative methane change calculated from realizations of GIP and GIP differences are very close. Moreover, and more importantly, the values obtained from realizations are very close to wellbore productions

independently determined from the field. These results ensure that the material balance and the values simulated are correct, and give additional confidence on the simulation results beyond basic statistics and the Q–Q plots discussed previously.

3.2.2 Spatial Time-Lapsed Gas-in-Place and Gas-in-Place Change Results with Interpretations on the Effect of Faults from Realizations—Realizations that correspond to Q50 GIPs for each coal seam at initial, 1998, 2006, and 2011 time periods are given in Fig. 7. Fault traces (red lines), corresponding dates during the degasification cycle, and the outermost entries that outline the E1–E11 panels (Fig. 2) are shown in these realizations as well. The realizations given for initial conditions of coal showed maximum GIP amounts that were equal to or more than 2 MMscf, 4 MMscf, and 2 MMscf per 0.92 acre in the New Castle, Mary Lee/Blue Creek, and Jagger seams, respectively. However, locations of the high-methane areas were different in each seam and do not seem to be affected by faults. For instance, at the initial state before degasification, areas with high methane concentrations were near the E1–E3 panel locations in the New Castle seam, were in E5–E6 panels on the Southeast area corner in the Mary Lee/Blue Creek seam, and were more evenly distributed in the Jagger seam.

With the start of degasification in the 80s and improvement in the early 90s by drilling additional wells, changes in distribution of GIP with time and fault effects became more discernible. The realizations representing 1998 in Fig. 7 show that GIP decreased significantly in all coal seams and high-methane content areas shrunk in size. For instance, in the New Castle seam, the amount of gas in E1–E6 panels as well as E10–E11 panels decreased to the 1.6–1.8 MMscf range. In this seam, the high-GIP areas in E1–E3 panels almost disappeared, and the high-gas area above the panels and in the northeast corner of the area shrunk. Similar changes also occurred in the Jagger seam. However, more discernible changes occurred in the Mary Lee/Blue Creek seams. The northeast corner of the area outside the faults dramatically decreased in GIP. Also, the area between the faults in the southwest area depleted in gas; so did the E1–E11 panel areas. These areas correspond to the locations of highly productive wells and the locations where coal reservoir properties favored high gas production using vertical wells (Karacan 2013a). GIP realizations given in Fig. 7 for 2006 and 2011 for the New Castle, Mary Lee/Blue Creek, and Jagger coal seams show that GIP continued to decrease, especially in panel areas, between the faults in the southwest and southeast ends of the E9 and E10–E11 panels due to active wells.

Time-interval GIP realizations are shown in Fig. 8. The spatial GIP change in coal seams between the initial state and 1998 discussed in the previous paragraph correlate well with the Q50 realizations from simulations of GIP difference data. These realizations showed that the region outside of the faults in the northeast, and the E1–E6 panel areas were where most GIP-reductions due to degasification occurred. The northeast faults created a region separated from rest of the study area, indicating compartmentalizing of degasification. In this figure, Q50 realizations of 1998–2006 and 2006–2011 GIP changes show that the E1–E11 panel area continued to deplete in GIP in all coals, at a slower rate. However, there was no change in GIP outside of the northeast faults because boreholes had stopped production after 1998. Similarly, there was no change in GIP around the southeast corner of the study area in 2006–2011 possibly for the same reason.

Finally, the GIP in the coal seams in 2015 and the GIP change in these coal seams during 2011–2015 were simulated for forecasting purposes. The GIP values corresponding to 2015 were calculated using the reservoir parameters obtained from production forecasting; that is, once past production of wells are successfully history-matched, the resulting analytical function can be extended into the future to predict production and the state of the reservoir. Figure 9 shows Q50 realizations of these simulations. The GIP change was expected to be uniform except in the areas where degasification had stopped and was isolated by faults. These areas are shown in white in the lower row for the New Castle seam, Mary Lee/Blue Creek seam, and the Jagger seam. The 2015 maximum forecasted GIP will be around 1 MMscf per 0.92 acre in the New Castle seam to the left of the 3rd fault line from the left. Thus, mine workings in this region will be prone to increased emissions from the mine roof. In the Mary Lee/Blue Creek seam, forecasts show areas in the 2.5–3 MMscf per 0.92 acre in the same above region, within the E1–E6 panel area and also at the southeast corner of the area. These regions will likely create more emissions from the mining face. The Jagger seam, on the other hand, will be more uniform in methane quantity and floor emissions will be expected to be spatially constant.

3.2.3 Statistical and Quantile Analysis of Gas-in-Place Within Realizations—

The histograms given in Fig. 10 show cumulative GIPs, calculated by summing 14,030 grid values, based on 100 realizations for each date. These histograms show that each coal seam has different GIP within the 12,900-acre area shown in Fig. 2. Moreover, they show that GIPs in coal seams decrease progressively over time from their initial state at the start of degasification until 2011. The GIPs are forecast to further decrease as a result of continued degasification into 2015.

The histograms in Fig. 10 show that the Mary Lee/Blue Creek seam had the highest initial cumulative GIP varying between 37.5 Bcf and 42.5 Bcf. If there had been no degasification, these seams would generate an average 3 MMscf of methane per acre of mining. As a result of degasification, cumulative GIP decreased to an average of 27 Bcf in 2011 (~35 % decrease) and is expected to decrease to 24 Bcf (an additional 7 % decrease) in 2015. Similar observations can be made for the New Castle and Jagger seams, which are the source of roof and floor emissions, respectively. Thus, from a mining-emissions point of view, these three major seams should be interpreted together. The histograms in Fig. 10 show these three major seams are within the direct emission interval during mining with an average of 72 Bcf of methane within the study area initially. Without degasification, this would correspond to 5.6 MMscf per acre of mining. With degasification, the total GIP in these three coal seams decreased significantly to 56 Bcf (4.3 MMscf per acre) until 1998, and continued to decrease at a slower pace to 46 Bcf (3.6 MMscf per acre) in 2011 and to 43 Bcf (3.3 MMscf per acre) in 2015. Statistical results from these distributions are given in Table 5 to assess uncertainty. In order to determine these statistical measures and Q5, Q50, and Q95, the cumulative GIPs in the model area were determined by summing the GIP of 14,030 cells in each of the 100 realizations of each date. Next, cumulative GIP values calculated for each realization were ranked to determine the GIP values and corresponding realizations that give 5 %, 50 %, and 95 % of the distribution. Similar analyses have been performed for GIP difference realizations between consecutive dates as well. Table 5

quantitatively shows that cumulative GIPs in all coal seams and their decrease with time. For instance, the Q50 of cumulative GIPs in the New Castle seam, Mary Lee/Blue Creek seam, and Jagger seam are expected to decrease from initial amounts of 14.6 Bcf, 39.9 Bcf, and 16.9 Bcf, to 9.5 Bcf, 24.3 Bcf, and 10.7 Bcf in 2015, respectively. These values correspond to 395 Mscf, 1.2 MMscf, and 480 Mscf reductions in possible mine emissions from the same coals per acre of mining, respectively, as the result of degasification.

4 Summary and Conclusions

In this work, reservoir and fluid storage properties of the New Castle coal seam, Mary Lee/Blue Creek seam, and Jagger seam of Black Warrior Basin, Alabama, were determined from production history matching and production forecasting of degasification wellbores. These data were combined with isotherm and other important data to compute GIP and its change with time at borehole locations. Point-wise GIP data were used to generate time-lapsed training images using Voronoi decomposition. Filter-based multiple-point geostatistical simulations were used after optimizing pattern partitioning and prototype generation parameters. Performed simulations were used for mapping time-lapsed methane quantities as well as their uncertainties within the study area. Results showed that TIs generated using Voronoi decomposition on training image grids of the same size as grids of planned simulations can create data patterns and their statistics successfully. Also, optimizing FILTERSIM parameters prior to simulations using Q–Q plots improve the final results of filter simulation.

Quantitative results of modeling showed that the cumulative methane quantity within coals in the study area was reduced from an initial ~73 Bcf (median) to ~46 Bcf as of 2011. It is forecasted that there will be an additional ~2 Bcf reduction in methane quantity by 2015. The Q50 of cumulative GIPs in the New Castle seam, Mary Lee/Blue Creek seam, and Jagger seam are expected to decrease from initial amounts of 14.6 Bcf, 39.9 Bcf, and 16.9 Bcf, to 9.5 Bcf, 24.3 Bcf, and 10.7 Bcf by 2015, respectively. These values correspond to 395 Mscf, 1.2 MMscf, and 480 Mscf reductions in possible mine emissions from the same coals per acre of mining, respectively, as the result of degasification. Quantitative results of simulations compared with wellbore productions showed that material balance of GIP was very close for each of the cases suggesting the accuracy of the modeling methodology given in this paper and reliability of the presented GIP results. The GIP values, spatial distributions, and the uncertainties calculated for different quantile criteria are not only important for generic interest and for locating future degasification boreholes, but they are also crucially important for estimating methane emissions from the working face, floor, and roof of the operating mine. These methane emissions and associated uncertainties have direct relations with the amount of ventilation air to be provided to the mine, and thus they are important for the health and safety of the underground workforce. For instance, based on Q50 results, ~3.1 MMscf potential methane emission from all three coal layers will require 310 MMscf air to dilute it to ~1 % in mining of each 0.92-acre area.

Acknowledgments

We are grateful to Dr. Jianbing Wu of ConocoPhillips for reviewing an initial version of this paper and for making useful comments. Dr. Jack Pashin and Richard Carroll of the Alabama Geological Survey are appreciated for their

help in providing degasification well productions and well logs. We also thank Dr. Daniel Mikeš and the anonymous reviewer for reviewing this paper and for making insightful comments. The author's would further like to disclaim that the findings and conclusions in this paper are those of the authors and do not necessarily represent the views of the National Institute for Occupational Safety and Health (NIOSH). Mention of any company name, product, or software does not constitute endorsement by NIOSH or the US Geological Survey.

References

Arpat B, Caers J. Conditional simulation with patterns. Math Geol. 2007; 39:177–203.

Deutsch, CV.; Journel, AG. GSLIB geostatistical software library and user's guide. 2. Oxford University Press; New York: 1998. p. 369

Dougherty HN, Karacan CÖ. A new methane control and prediction software suite for longwall mines. Comput Geosci. 2011; 37:1490–1500.

Fekete Associates. FAST CBM Calgary. Alberta, Canada: 2012.

Gamma Design Software. GS^{+} version 9. Plainwell, Michigan: 2008.

Golden Software. Surfer™ 10. 2012. http://www.goldensoftware.com/products/surfer/surfer.shtml

Groshong RH, Pashin JC. Structural controls on fractured coal reservoirs in the southern Appalachian Black Warrior foreland basin. J Struct Geol. 2009; 31:874–886.

Guardiano, F.; Srivastava, RM. Multivariate geostatistics: beyond bivariate moments. In: Soares, A., editor. Proceedings of the 4th international geostatistics Congress. Vol. 1. Kluwer Academic; Dordrecht: 1992.

Heriawan MN, Koike L. Identifying spatial heterogeneity of coal resource quality in a multilayer coal deposit by multivariate geostatistics. Int J Coal Geol. 2008; 73:307–330.

Journel, AG. Geostatistics: roadblocks and challenges. In: Soares, A., editor. Proceedings of the 4th international geostatistics congress. Vol. 1. Kluwer Academic; Dordrecht: 1992.

Journel AG, Gundeso R, Gringarten E, Yao T. Stochastic modeling of a fluvial reservoir: a comparative review of algorithms. J Pet Sci Eng. 1998; 21:95–121.

Karacan CÖ. Evaluation of relative importance of coalbed methane reservoir parameters for prediction of methane inflow rates during mining of longwall development entries. Comput Geosci. 2008; 34:1093–1114.

Karacan CÖ. Production history matching to determine reservoir properties of important coal groups in Upper Pottsville formation, Brookwood and Oak Grove fields, Black Warrior Basin, Alabama. J Nat Gas Sci Eng. 2013a; 10:51–67.

Karacan CÖ. Integration of vertical and in-seam horizontal well production analyses with stochastic geostatistical algorithms to estimate pre-mining methane drainage efficiency from coal seams: Blue Creek seam, Alabama. Int J Coal Geol. 2013b; 114:96–113.

Karacan CÖ, Goodman GVR. Analyses of geological and hydrodynamic controls on methane emissions experienced in a Lower Kittanning coal mine. Int J Coal Geol. 2012; 98:110–127.

Karacan CÖ, Ulery J, Goodman GVR. A numerical evaluation on the effects of impermeable faults on degasification efficiency and methane emissions during underground coal mining. Int J Coal Geol. 2008; 75:195–203.

Karacan CÖ, Ruiz FA, Cotè M, Phipps S. Coal mine methane: a review of capture and utilization practices with benefits to mining safety and to greenhouse gas reduction. Int J Coal Geol. 2011; 86:121–156.

Karacan CÖ, Olea RA, Goodman GVR. Geostatistical modeling of gas emissions zone and its in-place gas content for Pittsburgh seam mines using sequential Gaussian simulation. Int J Coal Geol. 2012; 90–91:50–71.

Leuangthong, O.; Khan, KD.; Deutsch, CV. Solved problems in geostatistics. Wiley; Hoboken: 2008. p. 207

Mackie KR, Cooper CD. Landfill gas emission prediction using Voronoi diagrams and importance sampling. Environ Model Softw. 2009; 24:1223–1232.

McFall KS, Wicks DE, Kuuskra VA. A geologic assessment of natural gas from coal seams in the Warrior Basin of Alabama. GRI Topical Report. 1986; 86-0272:80.

Noack K. Control of gas emissions in underground coal mines. Int J Coal Geol. 1998; 35:57–82.

Olea RA. A practical primer on geostatistics. U.S. Department of the Interior. US Geological Survey, Open-File Report 2009-1103. 2009:346.

Olea RA. Special issue on geostatistical and spatiotemporal modeling of coal resources. Int J Coal Geol. 2013; 112:1.

Olea RA, Luppens JA, Tewalt SJ. Methodology for quantifying uncertainty in coal assessments with an application to a Texas lignite deposit. Int J Coal Geol. 2011; 85:78–90.

Pashin JC. Hydrodynamics of coalbed methane reservoirs in the Black Warrior Basin: key to understanding reservoir performance and environmental issues. Appl Geochem. 2007; 22:2257–2272.

Pashin JC. Variable gas saturation in coalbed methane reservoirs of the Black Warrior Basin: implications for exploration and production. Int J Coal Geol. 2010; 82:135–146.

Reddy D, Prasanta KJ. Initialization for K-means clustering using Voronoi diagram. Proc Technol. 2012; 4:395–400.

Remy, N.; Boucher, A.; Wu, J. Applied geostatistics with SGeMS, a user's guide. Cambridge University Press; Cambridge: 2009. p. 264

Saulsberry, JL.; Schafer, PS.; Schraufnagel, RA. Gas Research Institute Report GRI-94/0397. Chicago, Illinois: 1996. A guide to coalbed methane reservoir engineering.

Srivastava M. Geostatistics: a toolkit for data analysis, spatial prediction and risk management in the coal industry. Int J Coal Geol. 2013; 112:2–13.

Strebelle, S. PhD thesis. Stanford University; Stanford, CA: 2000. Sequential simulation drawing structures from training images; p. 187

Wackernagel, H. Multivariate geostatistics—an introduction with applications. 3. Springer; Berlin: 2010. p. 387

Webster, R.; Oliver, MA. Geostatistics for environmental scientists. 2. Wiley; West Sussex: 2007. p. 330

Wu J, Boucher A, Zhang T. A SGeMS code for pattern simulation of continuous and categorical variables: FILTERSIM. Comput Geosci. 2008a; 34:1863–1876.

Wu J, Zhang T, Journel A. Fast FILTERSIM simulation with score-based distance. Math Geosci. 2008b; 40:773–788.

Zhang T. Incorporating geological conceptual models and interpretations into reservoir modeling using multiple-point geostatistics. Earth Sci Front. 2008; 15:26–35.

Zhang T, Switzer P, Journel AG. Filter-based classification of training image patterns for spatial simulation. Math Geol. 2006; 38:63–80.

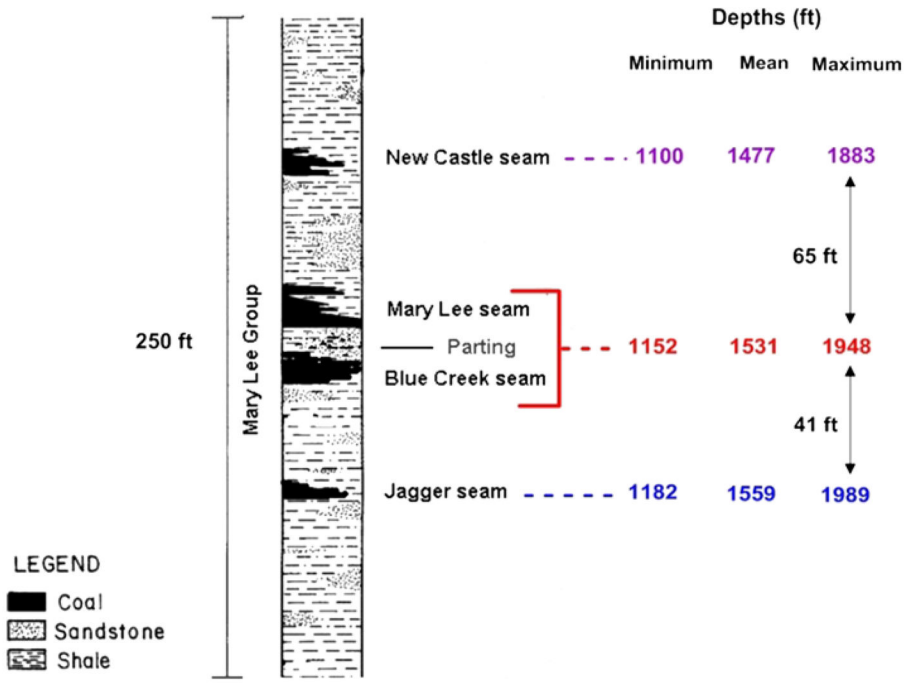

Fig. 1.

A representative stratigraphic column of the Mary Lee group of coals of the Upper Pottsville formation. The figure also shows minimum, mean, and maximum depths and inter-seam intervals within the study area

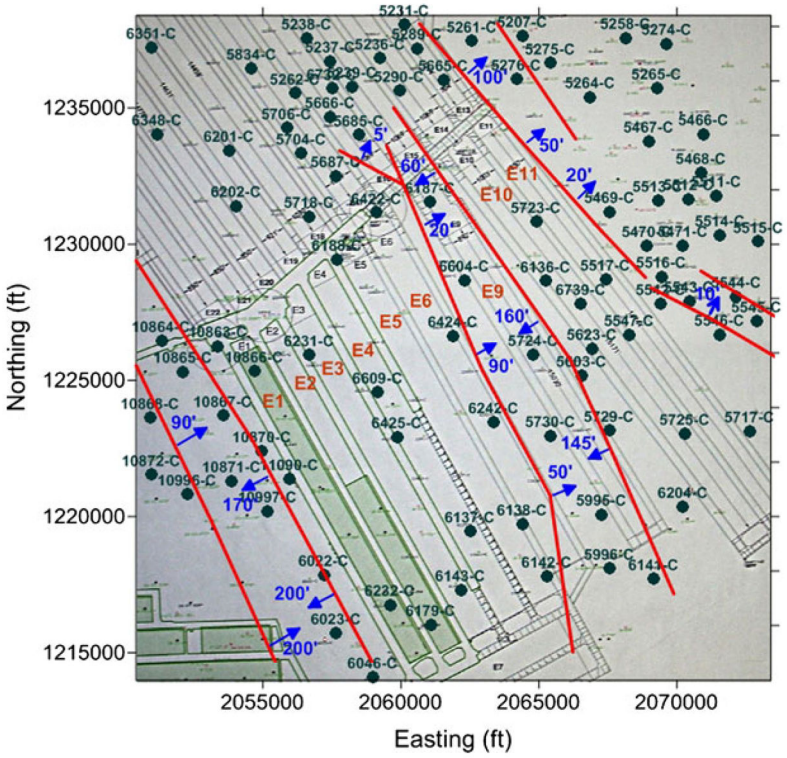

Fig. 2.

A plan view and dimensions of the study area with wellbore locations, mine outline, and major geologic structures. *Red lines* show normal faults mapped in the area and directions and magnitudes of throw. Locations of vertical boreholes and their identification numbers are also shown (*filled circles*) in this figure

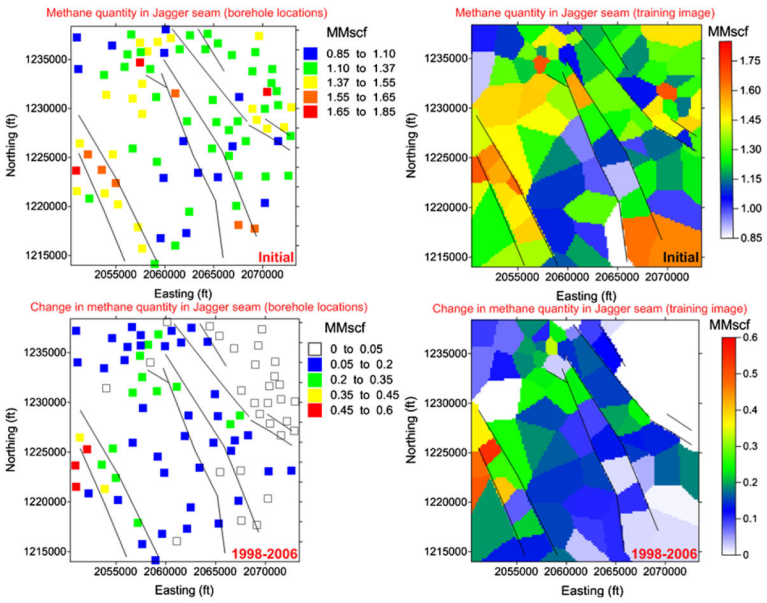

Fig. 3.

Spatial locations of data and faults for initial and difference (1998–2006) GIPs for the Jagger seam and the TIs generated for these cases. Easting and Northing coordinates are Alabama State coordinates of the study area. Twenty seven TIs were prepared to simulate each for the cases given in Tables 1 and 2

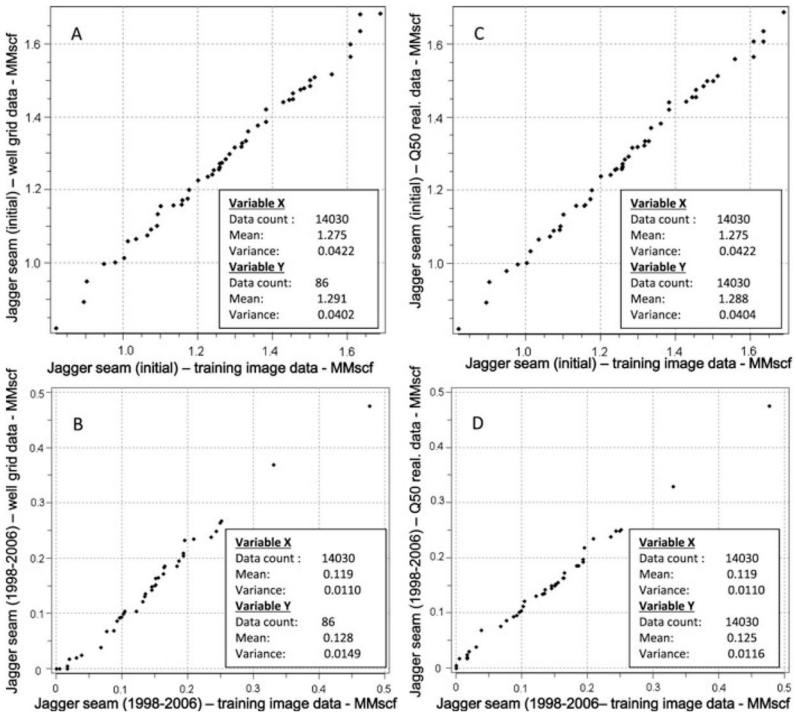

Fig. 4.

Q–Q plots of actual data and TIs prepared for initial and difference (1998–2006) GIPs for the Jagger seam (**A** and **B**) and Q–Q plots of Q50 realization data and TIs of the same attributes (**C** and **D**)

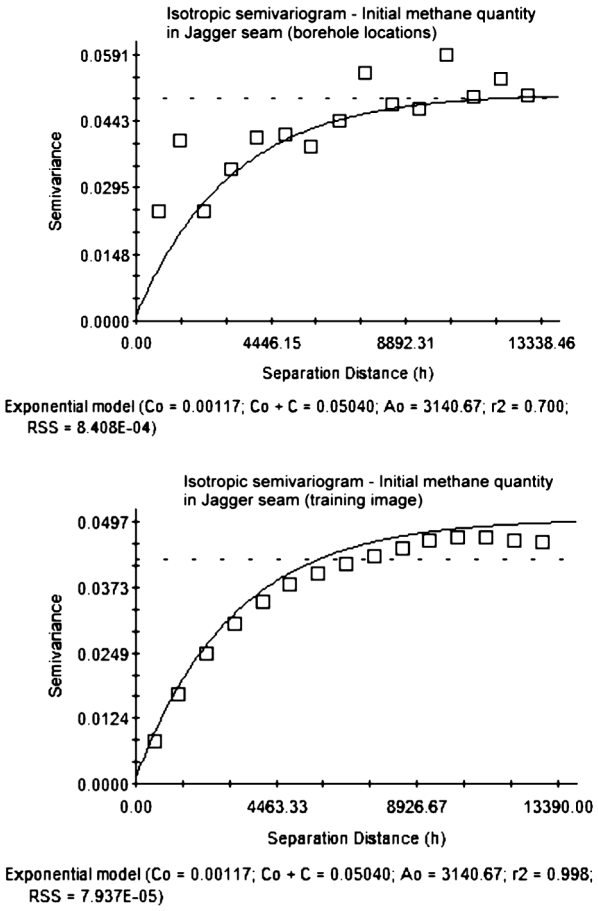

Fig. 5.

Comparison of the experimental and analytical semivariograms of Jagger seam's initial methane quantity from borehole locations and its TI given in Fig. 3

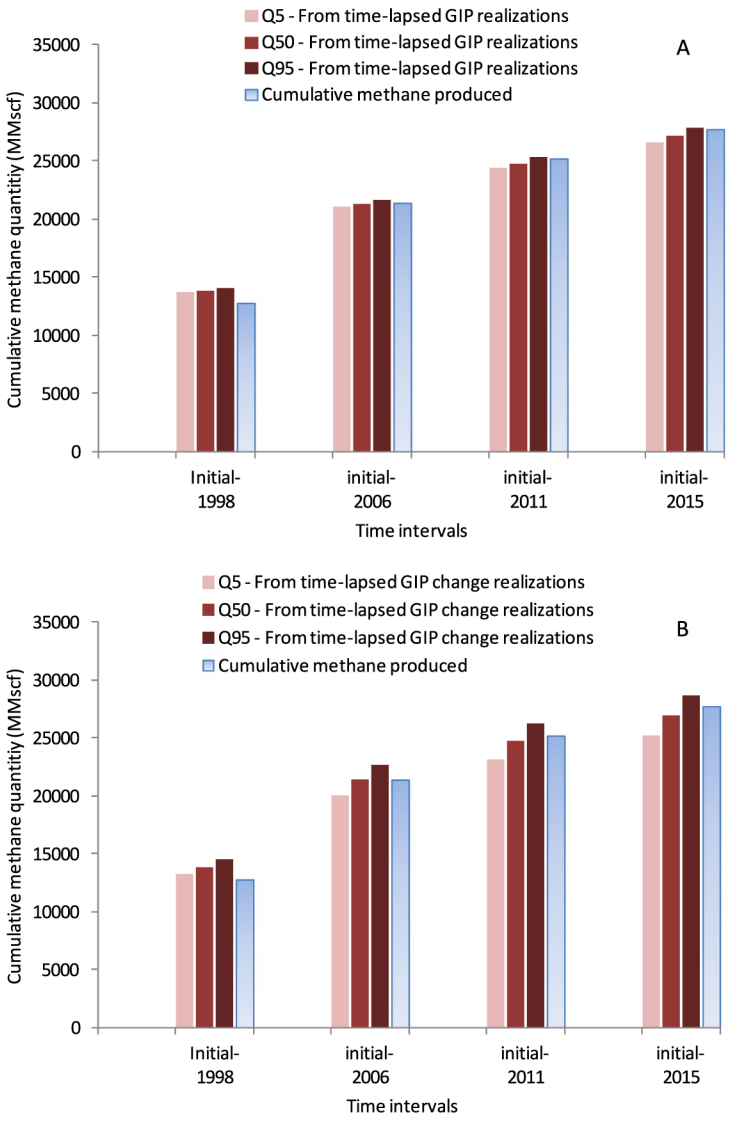

Fig. 6.

Cumulative methane produced from wellbores compared with the Q5, Q50, and Q95 of methane quantity change determined using time-lapsed GIP realizations (**A**) and time-lapsed GIP change realizations (**B**) between initial and later dates

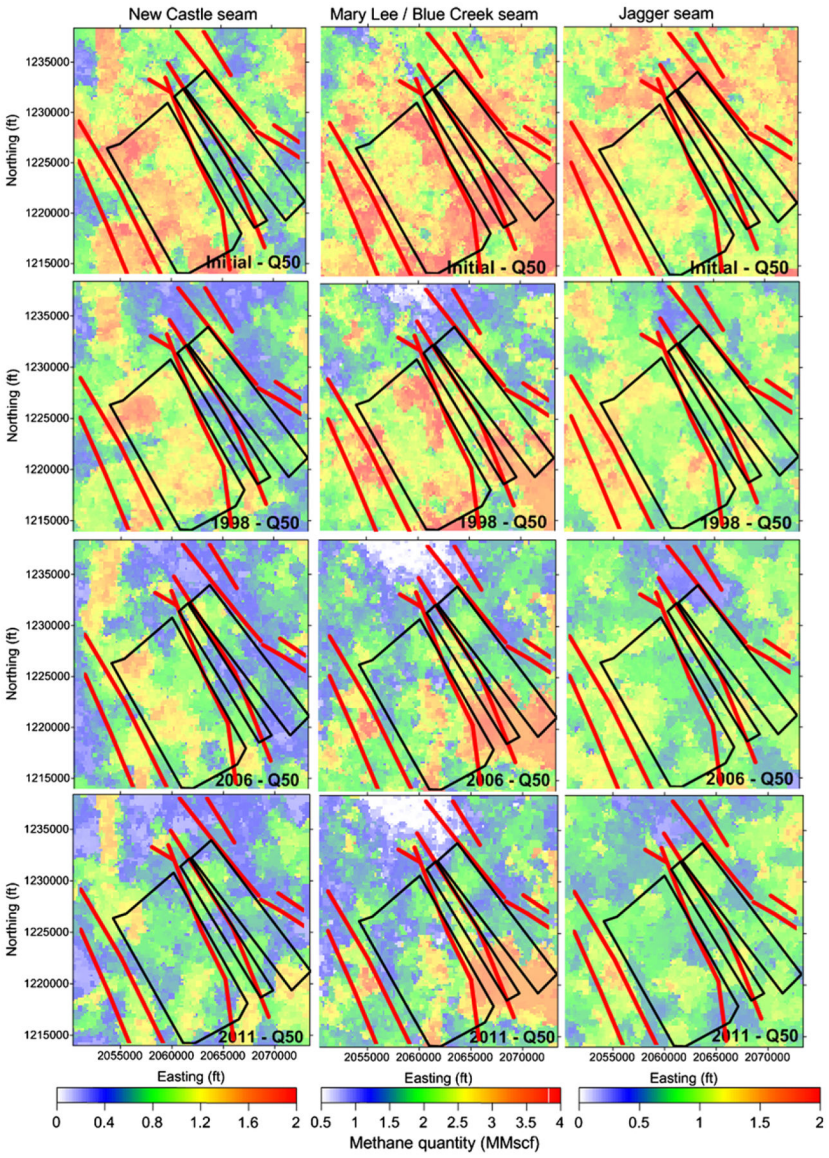

Fig. 7.

GIP realizations (Q50) of filter simulation results for each coal seam between initial and 2011. *Red lines* are fault lines and *black lines* are the outlines of E1–E11 panels

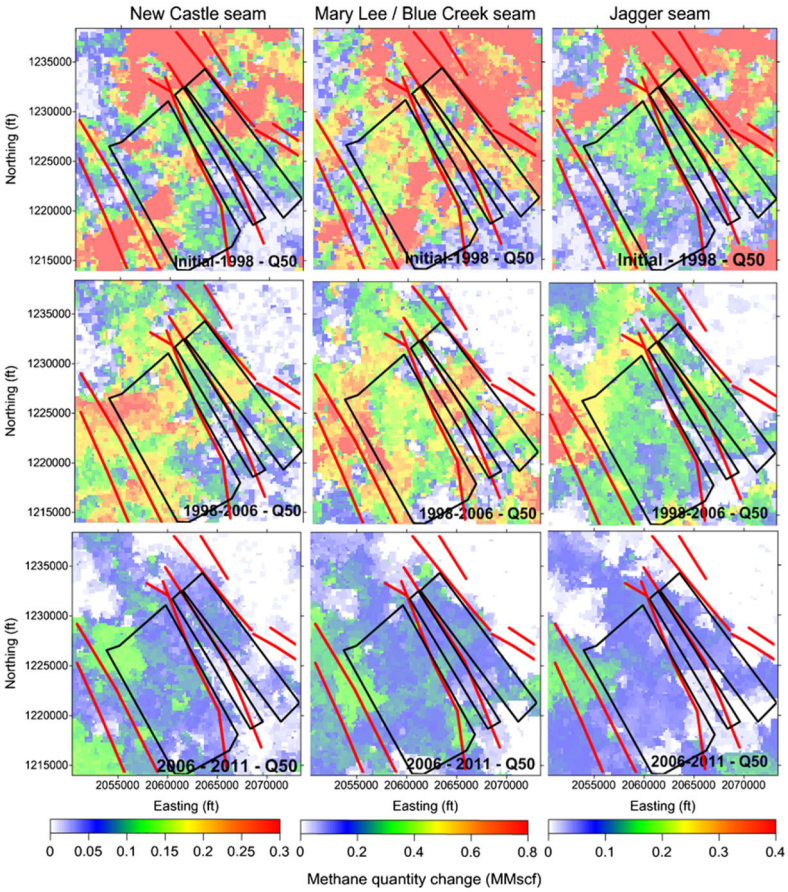

Fig. 8.

GIP change realizations (Q50) of coal seams within consecutive dates. *Red lines* are fault lines and *black lines* are the outlines of E1–E11 panels

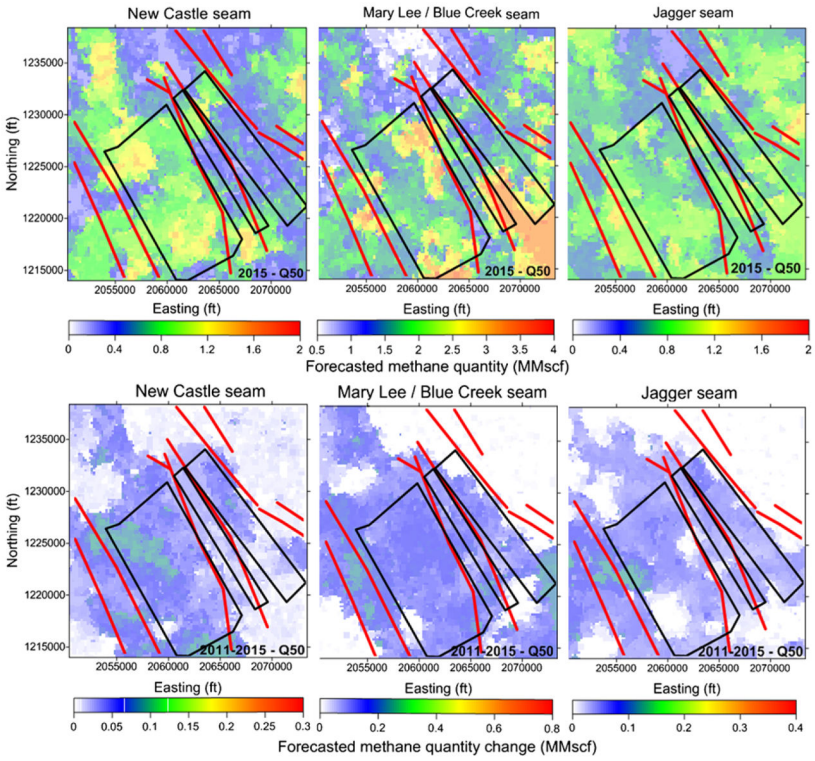

Fig. 9.

Forecasted GIPs in 2015 and GIP change between 2011 and 2015 in coal seams. *Color scales* are the same as in Fig. 7 and Fig. 8

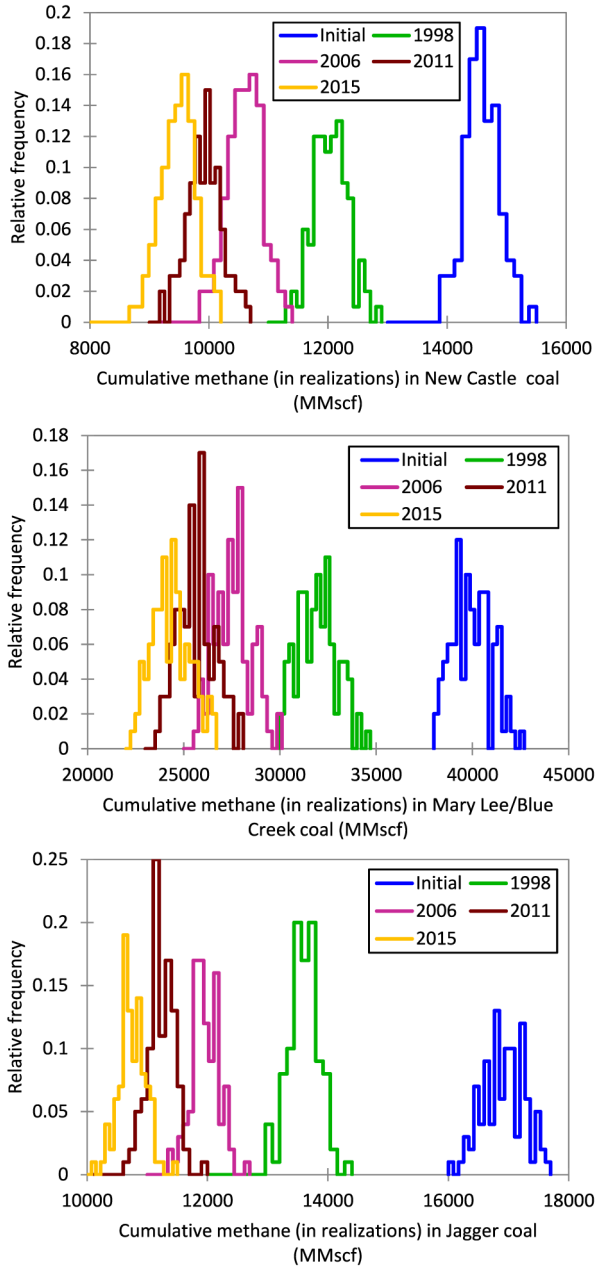

Fig. 10.

Cumulative GIP distributions, based on 100 realizations, in each coal seam from initial conditions to later dates

Table 1

GIP distribution statistics of 86 data points in each coal seam and at dates. “Initial” is condition of the coals prior to degasification and corresponds to dates 1987 and before

		Minimum	Maximum	Mean	Std. D.	Q5	Q50	Q95
New Castle seam (MMscf)	Initial	0.26	2.45	1.07	0.40	0.50	0.97	1.77
	1998	0.25	1.73	0.80	0.35	0.32	0.73	1.46
	2006	0.23	1.56	0.69	0.32	0.27	0.66	1.36
	2011	0.21	1.46	0.65	0.30	0.23	0.60	1.28
	2015	0.20	1.39	0.62	0.29	0.21	0.56	1.20
Mary Lee/Blue Creek seam (MMscf)	Initial	1.66	5.27	2.97	0.73	2.04	2.87	4.61
	1998	0.58	4.13	2.12	0.84	0.92	2.09	3.33
	2006	0.52	3.86	1.79	0.76	0.63	1.65	3.16
	2011	0.44	3.65	1.66	0.72	0.56	1.53	3.65
	2015	0.43	3.48	1.58	0.70	0.56	1.47	3.00
Jagger seam (MMscf)	Initial	0.82	1.69	1.29	0.20	0.98	1.28	1.64
	1998	0.32	1.60	0.97	0.28	0.56	0.95	1.40
	2006	0.30	1.45	0.84	0.25	0.41	0.82	1.27
	2011	0.26	1.45	0.79	0.25	0.39	0.77	1.19
	2015	0.25	1.45	0.76	0.25	0.39	0.72	1.17

Table 2

Statistics of GIP difference distributions in each coal seam between consecutive dates (statistics based on 86 data points). “Initial” is condition of the coals prior to degasification and corresponds to dates 1987 and before

		Minimum	Maximum	Mean	Std. D.	Q5	Q50	Q95
New Castle seam (MMscf)	Initial–1998	0.004	0.68	0.23	0.18	0.01	0.17	0.54
	1998–2006	0	0.30	0.10	0.08	0	0.10	0.23
	2006–2011	0	0.14	0.04	0.04	0	0.04	0.12
	2011–2015	0	0.09	0.03	0.03	0	0.03	0.08
Mary Lee/Blue Creek seam (MMscf)	Initial–1998	0.022	1.84	0.71	0.51	0.05	0.60	1.62
	1998–2006	0	1.40	0.33	0.30	0	0.31	0.86
	2006–2011	0	0.37	0.13	0.12	0	0.11	0.34
	2011–2015	0	0.24	0.08	0.08	0	0.08	0.21
Jagger seam (MMscf)	Initial–1998	0.006	0.97	0.31	0.25	0.01	0.22	0.77
	1998–2006	0	0.54	0.13	0.12	0	0.11	0.37
	2006–2011	0	0.17	0.05	0.05	0	0.05	0.15
	2011–2015	0	0.12	0.03	0.03	0	0.03	0.09

Table 3

GIP distribution statistics of TIs based on 14,030 grid cells in each coal seam and at pre-defined dates. As before, “initial” is the condition of the coals prior to degasification and corresponds to dates 1987 and before

		Minimum	Maximum	Mean	Std. D.	Q5	Q50	Q95
New Castle seam (MMscf)	Initial	0.26	2.45	1.15	0.47	0.50	1.08	2.10
	1998	0.25	1.73	0.89	0.37	0.31	0.66	1.22
	2006	0.23	1.56	0.77	0.33	0.29	0.74	1.37
	2011	0.21	1.46	0.73	0.32	0.23	0.69	1.30
	2015	0.20	1.39	0.70	0.31	0.23	0.68	1.26
Mary Lee/Blue Creek seam (MMscf)	Initial	1.66	5.27	3.16	0.79	2.04	3.02	4.75
	1998	0.58	4.13	2.40	0.83	0.94	2.43	3.97
	2006	0.52	3.86	2.05	0.76	0.73	1.91	3.21
	2011	0.44	3.65	1.91	0.74	0.73	1.75	3.21
	2015	0.43	3.48	1.82	0.73	0.73	1.65	3.21
Jagger seam(MMscf)	Initial	0.82	1.69	1.28	0.21	0.90	1.27	1.61
	1998	0.32	1.60	1.00	0.25	0.60	0.99	1.36
	2006	0.30	1.45	0.88	0.23	0.48	0.88	1.18
	2011	0.26	1.45	0.82	0.22	0.48	0.82	1.15
	2015	0.25	1.45	0.79	0.22	0.46	0.79	1.09

Table 4

Statistics of TI GIP difference distributions in each coal seam between consecutive dates (statistics based on 14,030 grid cells)

		Minimum	Maximum	Mean	Std. D.	Q5	Q50	Q95
New Castle seam (MMscf)	Initial–1998	0.004	0.68	0.18	0.17	0.00	0.13	0.53
	1998–2006	0	0.30	0.10	0.08	0.00	0.10	0.24
	2006–2011	0	0.14	0.05	0.04	0.00	0.05	0.12
	2011–2015	0	0.09	0.03	0.03	0.00	0.03	0.08
Mary Lee/Blue Creek seam (MMscf)	Initial–1998	0.022	1.84	0.58	0.49	0.03	0.50	1.63
	1998–2006	0	1.40	0.34	0.30	0.00	0.33	0.86
	2006–2011	0	0.37	0.14	0.11	0.00	0.15	0.35
	2011–2015	0	0.24	0.09	0.07	0.00	0.10	0.21
Jagger seam (MMscf)	Initial–1998	0.006	0.97	0.24	0.24	0.01	0.16	0.81
	1998–2006	0	0.54	0.12	0.11	0.00	0.11	0.26
	2006–2011	0	0.17	0.05	0.04	0.00	0.05	0.13
	2011–2015	0	0.12	0.04	0.03	0.00	0.04	0.09

Table 5

Basic statistics of cumulative GIP based on all 100 realizations, and Q5, Q50, and Q95, in the model area for all coal seams at each evaluation time. “Initial” is the condition of the coals prior to degasification and corresponds to dates 1987 and before. Cumulative GIP distributions from these realizations are given in Fig. 10

		Minimum	Maximum	Mean	Std. D.	Q5	Q50	Q95
New Castle seam (MMscf)	Initial	13,953	15,403	14,581	291	14,054	14,555	15,061
	1998	11,361	12,807	12,046	292	11,574	12,043	12,553
	2006	9,882	11,334	10,604	291	10,089	10,600	11,105
	2011	9,198	10,642	9,931	293	9,391	9,936	10,426
	2015	8,753	10,191	9,479	292	8,944	9,485	9,975
Mary Lee/Blue Creek seam (MMscf)	Initial	38,092	42,686	39,985	1,026	38,402	39,985	41,690
	1998	30,064	34,672	31,972	1,015	30,351	31,976	33,598
	2006	25,616	30,095	27,577	977	26,017	27,484	29,174
	2011	23,654	28,026	25,644	968	24,034	25,518	27,307
	2015	22,366	26,685	24,359	976	22,835	24,321	26,063
Jagger seam (MMscf)	Initial	16,003	17,649	16,918	342	16,332	16,924	17,467
	1998	12,996	14,367	13,606	249	13,109	13,606	13,959
	2006	11,351	12,684	11,960	230	11,558	11,939	12,315
	2011	10,603	11,953	11,229	225	10,850	11,214	11,566
	2015	10,145	11,482	10,747	224	10,366	10,733	11,059